Available online at www.sciencedirect.com
ScienceDirect
Journal of Power Sources 162 (2006) 667–672
JOURNAL OF POWER SOURCES
www.elsevier.com/locate/jpowsour

Short communication

Crystal chemistry and electrochemical characterization of layered $LiNi_{0.5-y}Co_{0.5-y}Mn_{2y}O_2$ and $LiCo_{0.5-y}Mn_{0.5-y}Ni_{2y}O_2$ ($0 \leq 2y \leq 1$) cathodes

J. Choi, A. Manthiram *

Materials Science and Engineering Program, The University of Texas at Austin, Austin, TX 78712, United States

Received 5 May 2006; received in revised form 14 June 2006; accepted 15 June 2006
Available online 27 July 2006

Abstract

The crystal chemistry and electrochemical performance of the layered $LiNi_{0.5-y}Co_{0.5-y}Mn_{2y}O_2$ and $LiCo_{0.5-y}Mn_{0.5-y}Ni_{2y}O_2$ oxide cathodes for $0 \leq 2y \leq 1$ have been investigated. Li_2MnO_3 impurity phase is observed for Mn-rich compositions with $2y > 0.6$ in $LiNi_{0.5-y}Co_{0.5-y}Mn_{2y}O_2$ and $2y < 0.2$ in $LiCo_{0.5-y}Mn_{0.5-y}Ni_{2y}O_2$. Additionally, the Ni-rich compositions encounter a volatilization of lithium at the high synthesis temperature of 900 °C. Compositions around $2y = 0.33$ are found to be optimum with respect to maximizing the capacity values and retention. The rate capabilities are found to bear a strong relationship to the cation disorder in the layered lattice. Moreover, the evolution of the X-ray diffraction patterns on chemically extracting lithium has revealed the presence of Li_2MnO_3 phase in addition to the layered phase for the composition $LiNi_{0.25}Co_{0.25}Mn_{0.5}O_2$ with an oxidation state of manganese close to 4+, which results in a large anodic peak at around 4.5 V due to the extraction of both lithium and oxygen.

Keywords: Lithium ion batteries; Layered oxides; Cation disorder; Crystal chemistry; Rate capability

1. Introduction

Layered $LiMO_2$ (M=Co, Ni, Mn and their solid solutions) oxides have been investigated widely as cathode materials for lithium-ion batteries due to their excellent electrode properties [1–3]. They exhibit high voltages arising from the highly oxidized $M^{3+/4+}$ redox couples, high capacity with a reversible extraction/insertion of theoretically one lithium ion per transition metal ion, high power density supported by the facile lithium extraction/insertion into the two-dimensional layered structure, and good electronic conductivity originating from the direct M–M interactions of the edge-shared MO_6 octahedra.

Recently, the layered $LiNi_{1-y-z}Mn_yCo_zO_2$ cathodes have become attractive due to their higher capacity, lower cost, and enhanced safety compared to the conventional $LiCoO_2$ cathode [4–8]. The high capacity of the layered $LiNi_{1-y-z}Mn_yCo_zO_2$ originates from the better chemical stability of the $Ni^{2+/3+}$ and $Ni^{3+/4+}$ redox couples compared to that of the $Co^{3+/4+}$ couple as has been demonstrated by our previous studies employing a chemical lithium extraction technique [9–11]. We presented recently a systematic electrochemical and structural characterizations of the layered $LiNi_{0.5y}Mn_{0.5-y}Co_{2y}O_2$ oxides for the entire range of $0 \leq 2y \leq 1$ [12]. The study revealed that the compositions with an optimum Co content of $0.33 \leq 2y \leq 0.5$ in $LiNi_{0.5-y}Mn_{0.5-y}Co_{2y}O_2$ exhibit high capacity with good cyclability, but the rate capability decreases with decreasing Co content due to an increasing cation disorder and consequent slow lithium extraction rate. We present here the synthesis, crystal chemistry, and electrochemical characterization of the analogous $LiNi_{0.5-y}Co_{0.5-y}Mn_{2y}O_2$ and $LiCo_{0.5-y}Mn_{0.5-y}Ni_{2y}O_2$ for $0 \leq 2y \leq 1$ and a comparison of the data with those of the $LiNi_{0.5-y}Mn_{0.5-y}Co_{2y}O_2$ system.

2. Experimental

The $LiNi_{0.5-y}Co_{0.5-y}Mn_{2y}O_2$ ($0 \leq 2y \leq 0.8$) and $LiCo_{0.5-y}Mn_{0.5-y}Ni_{2y}O_2$ ($0 \leq 2y \leq 0.58$) samples were prepared by firing required amounts of the coprecipitated hydroxides of Ni, Mn, and Co with 7 at.% excess lithium hydroxide in air at 900 °C for 24 h with a heating/cooling rate of 1 °C min^{-1}, excepting $LiNiO_2$ that was prepared by firing in O_2 atmosphere at 750 °C

* Corresponding author. Tel.: +1 512 471 1791; fax: +1 512 471 7681.
E-mail address: rmanth@mail.utexas.edu (A. Manthiram).

0378-7753/$ – see front matter © 2006 Elsevier B.V. All rights reserved.
doi:10.1016/j.jpowsour.2006.06.031

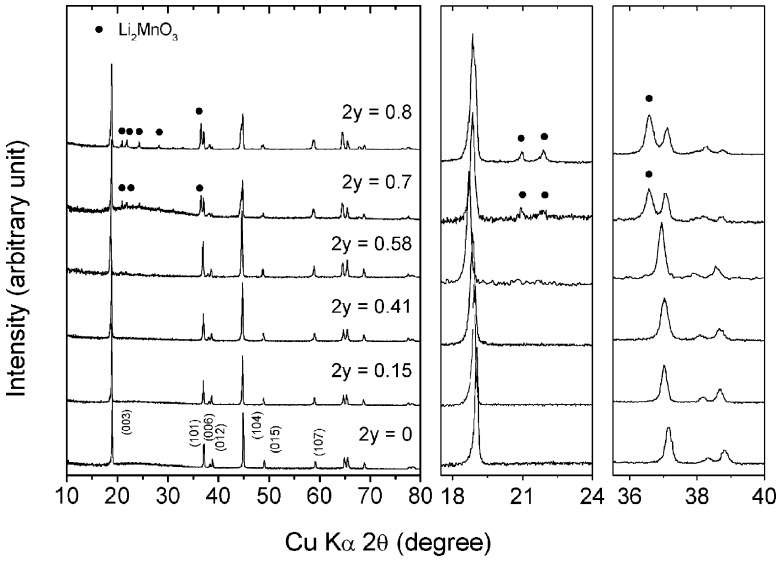

Fig. 1. X-ray diffraction patterns of $LiNi_{0.5-y}Co_{0.5-y}Mn_{2y}O_2$ for $0 \le 2y \le 0.8$.

for 24 h. The coprecipitated hydroxide precursors were obtained by adding an aqueous solution containing required amounts of Ni^{2+}, Mn^{2+}, and Co^{2+} into LiOH solution. Chemical extraction of lithium was carried out by stirring the powders in an acetonitrile solution of NO_2BF_4 for 2 days under argon atmosphere using a Schlenk line, followed by washing the products several times with acetonitrile under argon atmosphere to remove $LiBF_4$, drying under vacuum at ambient temperature, and storing in an argon-filled glove box to avoid reaction with the atmosphere.

All the samples were characterized by X-ray diffraction and the structural refinements and lattice parameter determinations were carried out with the Rietveld method using the DBWS-9411 PC program [13]. Lithium contents were determined by atomic absorption spectroscopy. Cathodes for evaluating the electrochemical performances were prepared by mixing 75 wt.% active material with 20 wt.% acetylene black and 5 wt.% PTFE binder, rolling the mixture into thin sheets of about 0.1 mm thick, and cutting into circular electrodes of 0.65 cm^2 area. CR2032 coin cells were then assembled with the cathode thus fabricated, lithium anode, and 1 M $LiPF_6$ in ethylene carbonate (EC)/diethyl carbonate (DEC) electrolyte.

3. Results and discussion

3.1. Crystal chemistry

Figs. 1 and 2 show the X-ray diffraction patterns of the $LiNi_{0.5-y}Co_{0.5-y}Mn_{2y}O_2$ and $LiCo_{0.5-y}Mn_{0.5-y}Ni_{2y}O_2$ samples, respectively. Impurity phases like Li_2MnO_3 are observed for Mn-rich compositions with $2y > 0.6$ in $LiNi_{0.5-y}Co_{0.5-y}Mn_{2y}O_2$ (Fig. 1) and $2y < 0.2$ in $LiCo_{0.5-y}Mn_{0.5-y}Ni_{2y}O_2$ (Fig. 2), while single phase layered oxides have been observed before for the entire range of $0 \le 2y \le 1$ in the analogous $LiNi_{0.5-y}Mn_{0.5-y}Co_{2y}O_2$ system [12].

Tables 1 and 2 give the lithium contents determined by atomic absorption spectroscopy in the $LiNi_{0.5-y}Co_{0.5-y}Mn_{2y}O_2$ and $LiCo_{0.5-y}Mn_{0.5-y}Ni_{2y}O_2$ samples. While the lithium contents remain slightly above 1.0 as the samples were synthesized with 7 at.% excess lithium for nickel contents $\le$0.33, a significant lithium deficiency is found for nickel-rich samples (nickel contents >0.33) in both the series. The lithium deficiency in the nickel-rich compositions when they are synthesized at high temperatures is a well-known phenomenon and it is due to the tendency of Ni^{3+} to get reduced to Ni^{2+} at high temperatures and a consequent volatilization of lithium oxide [14]. However, our previous study shows that the $LiNi_{0.5-y}Mn_{0.5-y}Co_{2y}O_2$ series of oxides synthesized at 900 °C do not lose much lithium since all the nickel is already present as Ni^{2+} (both Mn and Co are present as Mn^{4+} and Co^{3+}) in these compositions [12].

Table 1 summarizes the Rietveld analysis results of the $LiNi_{0.5-y}Co_{0.5-y}Mn_{2y}O_2$ samples carried out with the DBWS-

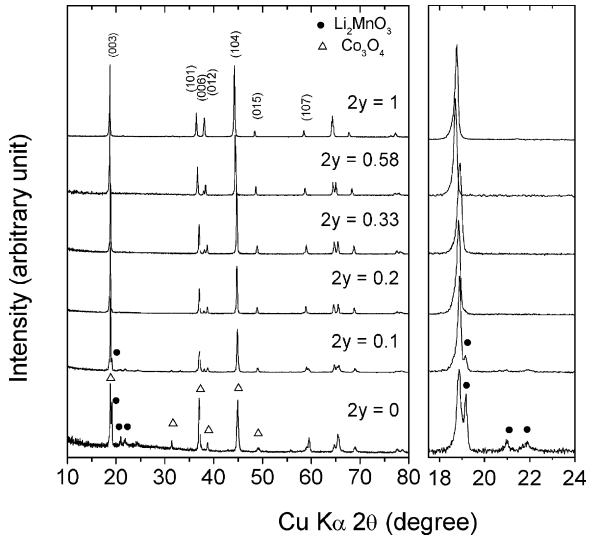

Fig. 2. X-ray diffraction patterns of $LiCo_{0.5-y}Mn_{0.5-y}Ni_{2y}O_2$ for $0 \le 2y \le 1$.

Table 1
Summary of the Rietveld analysis results of the layered $LiNi_{0.5-y}Co_{0.5-y}Mn_{2y}O_2$ ($0 \le 2y \le 1$) samples

$2y$	Li content	Lattice parameters				Thermal parameter, B_{Li} (Å^2)	Cation disorder (z) (%)
		a (Å)	c (Å)	V (Å^3)	c/a		
0	0.90	2.8526(1)	14.1596(6)	99.78	4.964	−5.590	5.7%
0.05	0.94	2.8568(1)	14.1865(5)	100.3	4.966	−5.328	7.3%
0.1	0.95	2.8583(1)	14.2003(7)	100.5	4.968	−4.653	5.6%
0.15	0.90	2.8587(1)	14.2069(5)	100.5	4.970	−3.306	3.5%
0.33	1.08	2.8562(1)	14.2045(4)	100.4	4.973	−1.741	3.0%
0.41	1.06	2.8536(1)	14.2061(7)	100.2	4.978	−2.019	2.4%
0.5	1.08	2.8535(1)	14.2242(8)	100.3	4.985	−0.054	1.7%
0.58	1.08	2.8494(1)	14.2173(12)	100.0	4.990	0.197	–
0.7	–	+ Li_2MnO_3					
0.8	–	+ Li_2MnO_3					

9411 PC program [13]. The data show that the a lattice parameter and the unit cell volume increase first and then decrease with increasing Mn content $2y$. Calculation of the valence states of the transition metal ions in the $LiNi_{0.5-y}Co_{0.5-y}Mn_{2y}O_2$ compositions assuming cobalt and manganese exist as Co^{3+} and Mn^{4+} reveals that the amount of Ni^{2+}, which has a predominant control on the lattice parameter and unit cell volume due to its much larger ionic radius compared to those of Co^{3+} or Mn^{4+} ions, reaches a maximum at $2y = 0.33$, leading to a maximum unit cell volume around $2y = 0.33$. Additionally, the lithium deficiency occurring due to lithium volatilization in the $2y \le 0.15$ compositions and the associated reduction of Ni^{3+} into Ni^{2+} keeps the unit cell volume high even to slightly lower Mn contents in $LiNi_{0.5-y}Co_{0.5-y}Mn_{2y}O_2$.

The data in Table 1 also indicate that the nickel-rich $LiNi_{0.5-y}Co_{0.5-y}Mn_{2y}O_2$ samples show significant negative values of B_{Li} (thermal parameter) when the Rietveld analysis is carried out with a strictly two dimensional model, and the B_{Li} becomes increasingly negative with decreasing Mn or increasing Ni content, indicating the presence of excess electron density in the lithium planes of these samples [15]. Therefore, the refinement was then carried out with a second model of $[Li_{1-a}Ni_a]_{3a}(Ni_{1-y-z-a}Mn_yCo_zLi_a)_{3b}\{O_2\}_{6c}$ by allowing a fraction of Ni^{2+} ions to be present in the lithium plane. Due to a smaller size difference between Ni^{2+} (0.690 Å) and Li^+ (0.76 Å) compared to those between other transition metal ions and Li^+, only Ni^{2+} is expected to exist in the lithium plane, as has been confirmed by neutron diffraction studies [16,17]. The refinement results with the second model reveal that the mixing of cations between the lithium and transition metal planes decreases with increasing Mn content as seen in Table 1 due to the decreasing lithium deficiency.

Table 2 summarizes the Rietveld analysis results of the $LiCo_{0.5-y}Mn_{0.5-y}Ni_{2y}O_2$ samples. The data indicate that the lattice parameter and unit cell volume increase monotonically with increasing Ni content $2y$. As in the case of the $LiNi_{0.5-y}Co_{0.5-y}Mn_{2y}O_2$ samples, the amount of Ni^{2+} reaches a maximum at $2y = 0.33$, which leads to a maximum in the lattice parameter and unit cell volume at $2y = 0.33$. However, as mentioned earlier, a significant lithium loss for $2y > 0.33$ in the $LiCo_{0.5-y}Mn_{0.5-y}Ni_{2y}O_2$ samples and the associated reduction of Ni^{3+} ions to Ni^{2+} at higher temperatures lead to a higher lattice parameter and unit cell volume even to higher Ni contents in this series. The % cation disorder in this series of samples was also obtained using the same method we used for the $LiNi_{0.5-y}Co_{0.5-y}Mn_{2y}O_2$ series, and the data show that the cation disorder increases with increasing Ni content in $LiCo_{0.5-y}Mn_{0.5-y}Ni_{2y}O_2$.

3.2. Electrochemical performance

Fig. 3 compares the initial discharge capacities and cyclabilites of the various $LiNi_{0.5-y}Co_{0.5-y}Mn_{2y}O_2$ samples cycled between 3.0 and 4.5 V at $C/5$ rate up to 50 cycles. While the capacity retentions get better with increasing Mn content $2y$, the capacity value decreases with increasing Mn content $2y$,

Table 2
Summary of the Rietveld analysis results of the layered $LiCo_{0.5-y}Mn_{0.5-y}Ni_{2y}O_2$ ($0 \le 2y \le 1$) samples

$2y$	Li content	Lattice parameters				Thermal parameter, B_{Li} (Å^2)	Cation disorder (z) (%)
		a (Å)	c (Å)	V (Å^3)	c/a		
0	–	$Co_3O_4 + Li_2MnO_3$					
0.1	–	+Li_2MnO_3					
0.2	1.07	2.8521(1)	14.2410(5)	100.3	4.993	−0.381	1.3%
0.33	1.08	2.8562(1)	14.2045(4)	100.4	4.973	−1.741	3.0%
0.41	0.97	2.8613(1)	14.2060(5)	100.7	4.965	−3.121	3.7%
0.5	0.92	2.8676(1)	14.2148(6)	101.2	4.957	−4.782	6.5%
0.58	0.75	2.8742(1)	14.2429(4)	101.9	4.955	−3.567	4.9%
1	0.98	2.8919(1)	14.2292(4)	103.1	4.920	−7.394	14.4%

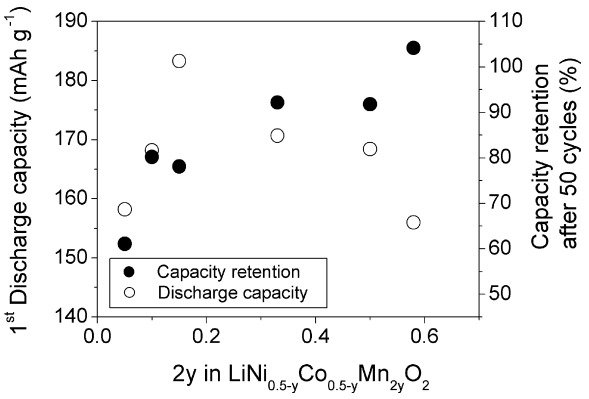

Fig. 3. Comparison of the first discharge capacities and capacity retentions of the layered $LiNi_{0.5-y}Co_{0.5-y}Mn_{2y}O_2$ cathodes. The data were collected between 3.0 and 4.5 V at *C*/5 rate up to 50 cycles.

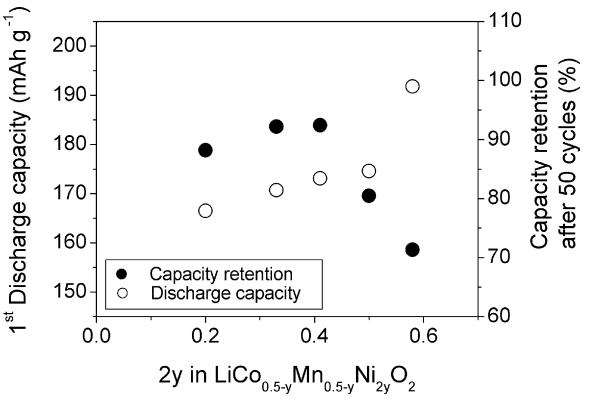

Fig. 5. Comparison of the first discharge capacities and capacity retentions of layered $LiCo_{0.5-y}Mn_{0.5-y}Ni_{2y}O_2$ cathodes. The data were collected between 3.0 and 4.5 V at *C*/5 rate up to 50 cycles.

resulting in an optimum composition range of $0.33 \leq 2y \leq 0.5$ with around 170 mAh g^{-1} and over 90% capacity retention. Interestingly, the capacity retention data indicate that the $LiNi_{0.21}Co_{0.21}Mn_{0.58}O_2$ sample has slightly higher discharge capacity in the 50th cycle compared to the first cycle. This increase in capacity on cycling could be explained by considering the change in the shape of the discharge profile with cycle number (Fig. 4). Fig. 4a reveals that $LiNi_{0.21}Co_{0.21}Mn_{0.58}O_2$ has a discharge profile similar to those of the cobalt-rich composition $LiNi_{0.21}Mn_{0.21}Co_{0.58}O_2$ (Fig. 4b) and the nickel-rich composition $LiCo_{0.21}Mn_{0.21}Ni_{0.58}O_2$ (Fig. 4c), with a steep

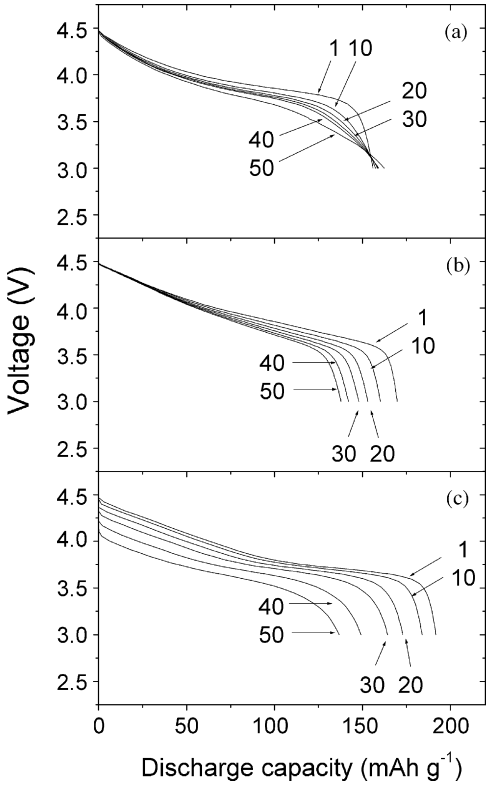

Fig. 4. Comparison of the discharge profiles at various cycle numbers of (a) $LiNi_{0.21}Co_{0.21}Mn_{0.58}O_2$, (b) $LiNi_{0.21}Mn_{0.21}Co_{0.58}O_2$, and (c) $LiCo_{0.21}Mn_{0.21}Ni_{0.58}O_2$. The data were collected between 3.0 and 4.5 V at *C*/5 rate up to 50 cycles.

profile below 3.5 V during its first discharge. However, while the steep discharge profiles below 3.5 V are maintained by the other compositions on cycling, the discharge profile of $LiNi_{0.21}Co_{0.21}Mn_{0.58}O_2$ below 3.5 V becomes more and more sloping with increasing cycle number, leading to a higher discharge capacity at higher number of cycles.

Fig. 5 compares the initial discharge capacities and cyclabilites of the various $LiCo_{0.5-y}Mn_{0.5-y}Ni_{2y}O_2$ samples cycled between 3.0 and 4.5 V at *C*/5 rate up to 50 cycles. While the discharge capacity generally increases with increasing Ni content 2*y*, the capacity retention is maximized (> 90% retention) in the compositional range of $0.33 \leq 2y \leq 0.41$. Outside this range with $2y < 0.33$ or > 0.41, the capacity retention of the $LiCo_{0.5-y}Mn_{0.5-y}Ni_{2y}O_2$ samples falls below 90%. Fig. 4c compares the discharge profiles of $LiCo_{0.21}Mn_{0.21}Ni_{0.58}O_2$ at various cycle numbers. The data suggest that the significant capacity fade in the nickel-rich compositions may be related to the large impedance development during cycling compared to those with the cobalt-rich (Fig. 4b) and manganese-rich compositions (Fig. 4a); the impedance development is evident from the decrease in the discharge voltage as the sample is cycled in Fig. 4c. The increase in impedance may be related to the structural instability arising from a migration of nickel from the transition metal plane to the lithium plane via the neighboring tetrahedral sites [18,19].

With an aim to confirm the correlation between the cation disorder and rate capability, as was seen in the $LiNi_{0.5-y}Mn_{0.5-y}Co_{2y}O_2$ system [12], we have studied the rate capabilities of the $LiNi_{0.5-y}Co_{0.5-y}Mn_{2y}O_2$ and $LiCo_{0.5-y}Mn_{0.5-y}Ni_{2y}O_2$ cathodes as well by discharging them at various *C*-rates from *C*/10 to 4*C* between 4.3 and 3.0 V (Fig. 6). A lower cutoff charge voltage of 4.3 V compared to the 4.5 V used in the cyclability tests was chosen to minimize the effects of any capacity degradation that may occur due to poor cycling properties at higher cutoff voltages. The data in Fig. 6 reveal that the rate capability decreases with decreasing Mn content in the $LiNi_{0.5-y}Co_{0.5-y}Mn_{2y}O_2$ system and with increasing Ni content in the $LiCo_{0.5-y}Mn_{0.5-y}Ni_{2y}O_2$ system due to an increasing cation disorder as seen in Tables 1 and 2. The data thus establish

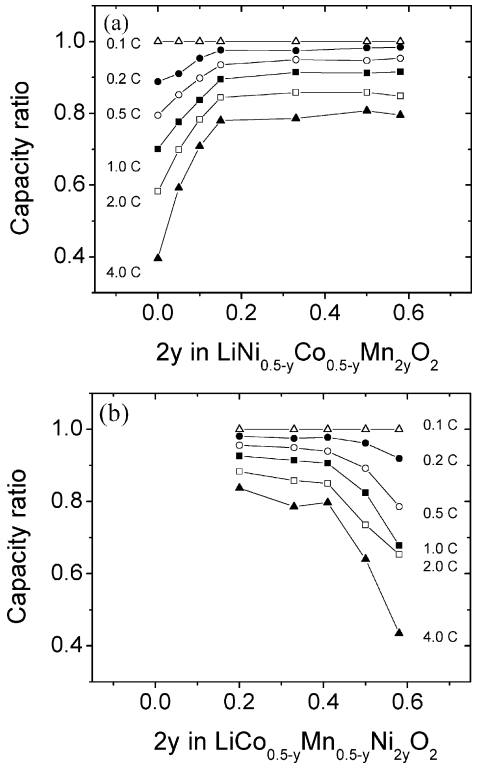

Fig. 6. Comparison of the rate capabilities of (a) $LiNi_{0.5-y}Co_{0.5-y}Mn_{2y}O_2$ and (b) $LiCo_{0.5-y}Mn_{0.5-y}Ni_{2y}O_2$ cathodes. The capacity ratio values were obtained by dividing the discharge capacity at various *C* rates by the discharge capacity at 0.1 C rate.

a clear relationship between cation disorder and rate capability in the layered $LiNi_{1-y-z}Co_yMn_zO_2$ systems, consistent with our previous data with the $LiNi_{0.5-y}Mn_{0.5-y}Co_{2y}O_2$ system [12].

3.3. $LiNi_{0.25}Co_{0.25}Mn_{0.5}O_2$

Fig. 7 compares the X-ray diffraction patterns of the $Li_{1-x}Ni_{0.25}Co_{0.25}Mn_{0.5}O_2$ samples that were obtained by chemically extracting lithium from $LiNi_{0.25}Co_{0.25}Mn_{0.5}O_2$ with NO_2BF_4 in acetonitrile medium. As lithium is extracted, the *a* and *c* lattice parameters of the initial O3 type phase having an oxygen stacking sequence of ABCABC along the *c* axis [20] changes, and additional reflections corresponding to a second phase is seen at $(1-x)=0.45$. This second phase is identified as Li_2MnO_3 with all the manganese existing as Mn^{4+}. With further lithium extraction, the samples with $(1-x)<0.25$ consist of a layered O1 type phase having an oxygen stacking sequence of ABABAB along the *c* axis and the Li_2MnO_3 phase. The formation of the layered O1 type phase from the initial O3 type phase at low lithium contents is consistent with our previous findings for systems having a moderate amount of cation disorder such as $LiNi_{1/3}Mn_{1/3}Co_{1/3}O_2$ [12,21]. The data in Fig. 7 suggests that the initial $LiNi_{0.25}Co_{0.25}Mn_{0.5}O_2$ sample consists of two phases, a layered O3 type phase and the Li_2MnO_3 phase, but a overlap of the reflections corresponding to the two phases makes it difficult to recognize the presence of Li_2MnO_3 phase in the initial $LiNi_{0.25}Co_{0.25}Mn_{0.5}O_2$ sample.

Fig. 8 compares the cyclic voltammograms (first cycle) of the $LiCo_{0.25}Mn_{0.25}Ni_{0.5}O_2$, $LiNi_{0.25}Mn_{0.25}Co_{0.5}O_2$, and $LiNi_{0.25}Co_{0.25}Mn_{0.5}O_2$ samples. The data reveal that a large irreversible anodic peak at around 4.5 V can be found mainly for the manganese-rich composition ($LiNi_{0.25}Co_{0.25}Mn_{0.5}O_2$). This observation is usually attributed to the simultaneous extraction of lithium and oxygen from the manganese-rich compositions of the layered $LiNi_xLi_{1/3-2x/3}Mn_{2/3-x/3}O_2$ system ($x<1/2$) [22] since it is difficult to oxidize manganese ions beyond Mn^{4+}. It is reasonable to expect the valence of manganese to be 3.5+ in the $LiNi_{0.25}Co_{0.25}Mn_{0.5}O_2$ composition with all the nickel and cobalt existing as Ni^{2+} and Co^{3+}. With this, all the lithium could be extracted without having to oxidize the manganese beyond Mn^{4+}. However, the average oxidation state of the transition metal ions (Ni, Mn, Co) obtained by iodometric titration is found to be 3.18+, which is higher than the theoretically expected value of 3.0+ for the layered $LiMO_2$ oxide, indicating that the oxidation state of manganese is significantly higher than the

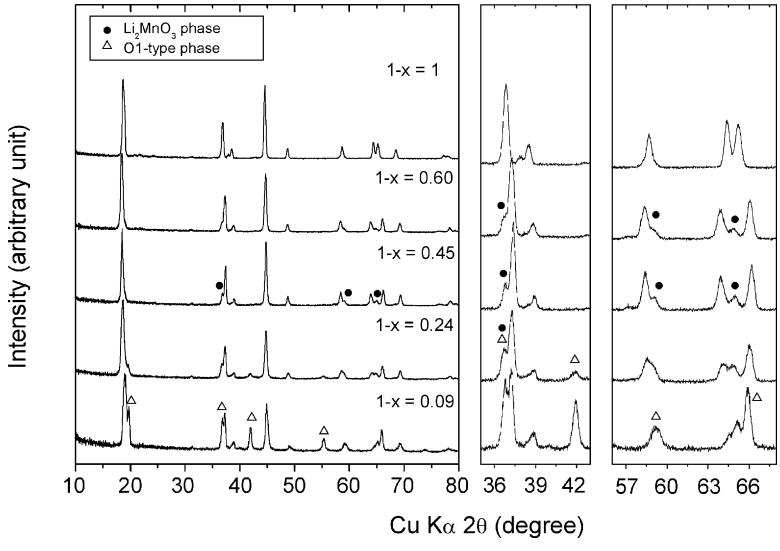

Fig. 7. X-ray diffraction patterns of the chemically delithiated $Li_{1-x}Ni_{0.25}Co_{0.25}Mn_{0.5}O_2$. The patterns on the right show an expansion of a small 2θ range.

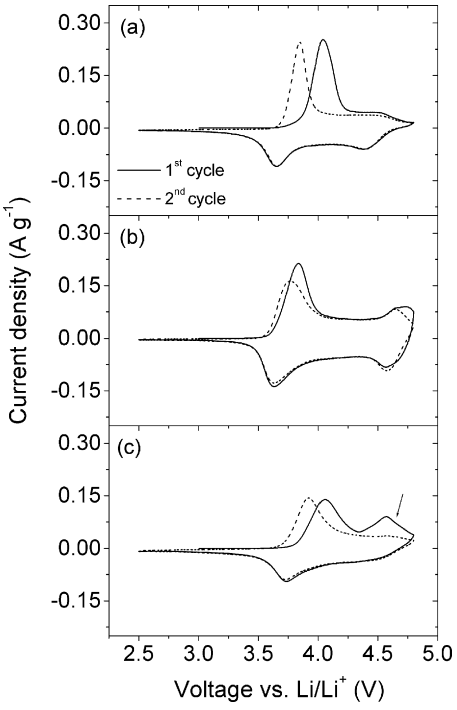

Fig. 8. Comparison of the cyclic voltammograms recorded between 2.5 and 4.8 V at 100 μV s^{-1}: (a) $LiCo_{0.25}Mn_{0.25}Ni_{0.5}O_2$, (b) $LiNi_{0.25}Mn_{0.25}Co_{0.5}O_2$, and (c) $LiNi_{0.25}Co_{0.25}Mn_{0.5}O_2$. Solid and dotted lines refer, respectively, to first and second cycles.

theoretically expected value of 3.5+ assuming nickel and cobalt exist as Ni^{2+} and Co^{3+}. The higher oxidation state of manganese is further supported by the X-ray diffraction data revealing the existence of a layered and a Li_2MnO_3 phase with Mn^{4+}. Thus the simultaneous extraction of lithium and oxygen or the extraction of lithium by oxidizing O^{2-} in $LiNi_{0.25}Co_{0.25}Mn_{0.5}O_2$ (i.e. extraction of lithium from the Li_2MnO_3 phase) seems to lead to the large anodic peak at around 4.5 V. Additionally, the improvement in capacity retention or the slight increase in capacity on cycling for the Mn-rich compositions, as seen in Figs. 3 and 4a, can be explained by considering the presence of the Li_2MnO_3 phase. Since the cutoff charge voltage of 4.5 V is high enough to extract lithium and oxygen simultaneously and generate electrochemically active Mn^{3+}, the Mn-rich compositions show an increasing capacity near 3 V with cycle number, resulting in a better cyclability at higher number of cycles.

4. Conclusions

The layered $LiNi_{0.5-y}Co_{0.5-y}Mn_{2y}O_2$ and $LiCo_{0.5-y}Mn_{0.5-y}Ni_{2y}O_2$ oxide cathodes have been synthesized and characterized. The nickel-rich compositions in both the series show a significant loss of lithium during synthesis at 900 °C, leading to poor cyclability and rate capability. The manganese-rich compositions in both the series suffer from the formation of the impurity phase Li_2MnO_3, resulting in a lower reversible capability. The optimum compositional range in the $LiNi_{1-y-z}Mn_yCo_zO_2$ system with respect to electrochemical performance is found to be around the $LiNi_{1/3}Mn_{1/3}Co_{1/3}O_2$ composition. Additionally, the $LiNi_{0.25}Co_{0.25}Mn_{0.5}O_2$ composition is found to consist of a Li_2MnO_3 phase in addition to the expected layered oxide phase as could be recognized from the chemical delithiation experiments. The presence of the Li_2MnO_3 phase and a significantly higher oxidation state of manganese (close to 4+) leads to a large anodic peak at around 4.5 V and a slightly better cyclability with increasing cycle number in the manganese rich compositions.

Acknowledgments

Financial support by the Office of FreedomCAR and Vehicle Technologies of the U.S. Department of Energy under Contract No. DE-AC03-76SF00098 (Subcontract No. 6712770) and the Welch Foundation grant F-1254 is gratefully acknowledged.

References

[1] A. Manthiram, in: C. Julien, J.P. Pereira-Ramos, A. Momchilov (Eds.), New Trends in Intercalation Compounds for Energy Storage, Kluwer Academic Publisher, The Netherland, 2002, p. 157.
[2] A. Manthiram, in: C. Julien, J.P. Pereira-Ramos, A. Momchilov (Eds.), New Trends in Intercalation Compounds for Energy Storage, Kluwer Academic Publisher, The Netherland, 2002, p. 176.
[3] T. Ohzuku, A. Ueda, Solid State Ionics 69 (1994) 201.
[4] Z. Liu, A. Yu, J.Y. Lee, J. Power Sources 81/82 (1999) 416.
[5] M. Yoshio, H. Noguchi, J. Itoh, M. Okada, T. Mouri, J. Power Sources 90 (2000) 176.
[6] T. Ohzuku, Y. Makimura, Chem. Lett. (2001) 642.
[7] N. Yabuuchi, T. Ohzuku, J. Power Sources 119–121 (2003) 171.
[8] J. Choi, A. Manthiram, Electrochem, Solid State Lett. 7 (2004) A365.
[9] R.V. Chebiam, F. Prado, A. Manthiram, Chem. Mater. 13 (2001) 2951.
[10] R.V. Chebiam, F. Prado, A. Manthiram, J. Solid State Chem. 163 (2002) 5.
[11] S. Venkatraman, A. Manthiram, Chem. Mater. 14 (2002) 3907.
[12] J. Choi, A. Manthiram, Solid State Ionics 176 (2005) 2251.
[13] R.A. Young, A. Shakthivel, T.S. Moss, C.O. Paiva Santos, J. Appl. Crystallogr. 28 (1995) 366.
[14] H. Arai, S. Okada, H. Ohtsuka, M. Ichimura, J. Yamaki, Solid State Ionics 80 (1995) 261.
[15] A. Rougier, P. Gravereau, C. Delmas, J. Electrochem. Soc. 143 (1996) 1168.
[16] Z. Lu, L.Y. Beaulie, R.A. Donaberger, C.L. Thomas, J.R. Dahn, J. Electrochem. Soc. 149 (2002) A778.
[17] H. Kobayashi, H. Sakaebe, H. Kageyama, K. Tatsumi, Y. Arachi, T. Kamiyama, J. Mater. Chem. 13 (2003) 590.
[18] R.V. Chebiam, F. Prado, A. Manthiram, J. Electrochem. Soc. 148 (2001) A49.
[19] S. Choi, A. Manthiram, J. Electrochem. Soc. 149 (2002) A1157.
[20] C. Delmas, C. Fouassier, P. Hagenmuller, Physica 99B (1980) 81.
[21] J. Choi, A. Manthiram, J. Mater. Chem. 16 (2006) 1726.
[22] Z. Lu, J.R. Dahn, J. Electrochem. Soc. 149 (2002) A815.